Article:
Gardner, R, Piazolo, S orcid.org/0000-0001-7723-8170, Evans, L et al. (1 more author) (2017) Patterns of strain localization in heterogeneous, polycrystalline rocks – a numerical perspective. Earth and Planetary Science Letters, 463. pp. 253-265. ISSN 0012-821X

https://doi.org/10.1016/j.epsl.2017.01.039

Appendix 1: Elle-Basil numerical model

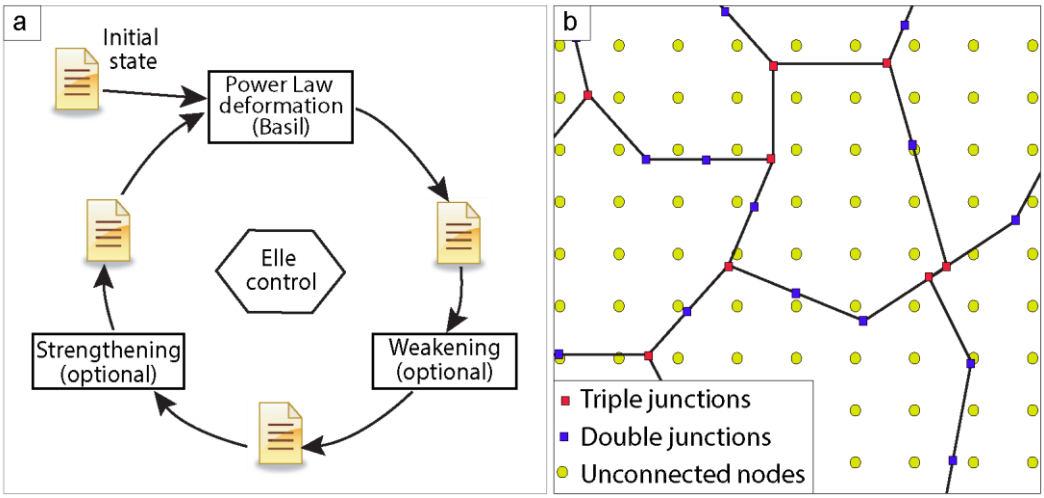

Supplementary Figure 1. Flow diagram of numerical model overview. (a) Control script controls each step of the numerical simulation, providing the input structure and deformation boundary conditions to the viscous deformation code (Basil) and then stepping through the other processes acting on the structure; (b) Elle layer 1 polygon geometry is defined by a mesh of interconnected boundary nodes represented by blue and red dots, for double and triple intersections, respectively, layer 2 is a regular mesh of unconnected nodes represented by yellow dots.

Appendix 2: Material strength bound calculation

Simulation set I: a mixed viscosity model has been used where weak polygons have viscosity of 1 and the strong polygons have viscosity of 5.

For the two component mixture the upper, iso-stress bound is calculated:

$$S_U = \alpha_1 S_1 + \alpha_2 S_2 \qquad \text{equation 1}$$

S is the strength for that component from the control models (Supplementary Table 1). The lower, iso-strain bound, is calculated:

$$S_L = 1/(\alpha_1/S_1 + \alpha_2/S_2) \qquad \text{equation 2}$$

The strength graph for Newtonian flow (Supplementary Figure 2a) shows the geometries all fall within the iso-stress and iso-strain bounds. The vertical geometry, at its strongest, approaches the iso-stress bound while the horizontal geometry approaches the iso-strain bound. The geometry with two horizontal stripes, as used in the numerical experiments, is marginally stronger than a single horizontal stripe. Both of these geometries use an irregular polygon mesh (Supp. Fig. 2b (i) and (ii)), and both are marginally stronger than the iso-strain bound (Supp. Fig. 2a, solid and dashed green lines). The edge irregularities were eliminated

to create a single stripe of “bricks”, (Supp. Fig. 2a, dotted green line and 2b (iii)). The strength of this geometry matches the iso-strain bound. A similar case holds for the vertical stripes. The marginal variation from the upper iso-stress bound is due to the irregularities of the edges of the vertical stripes.

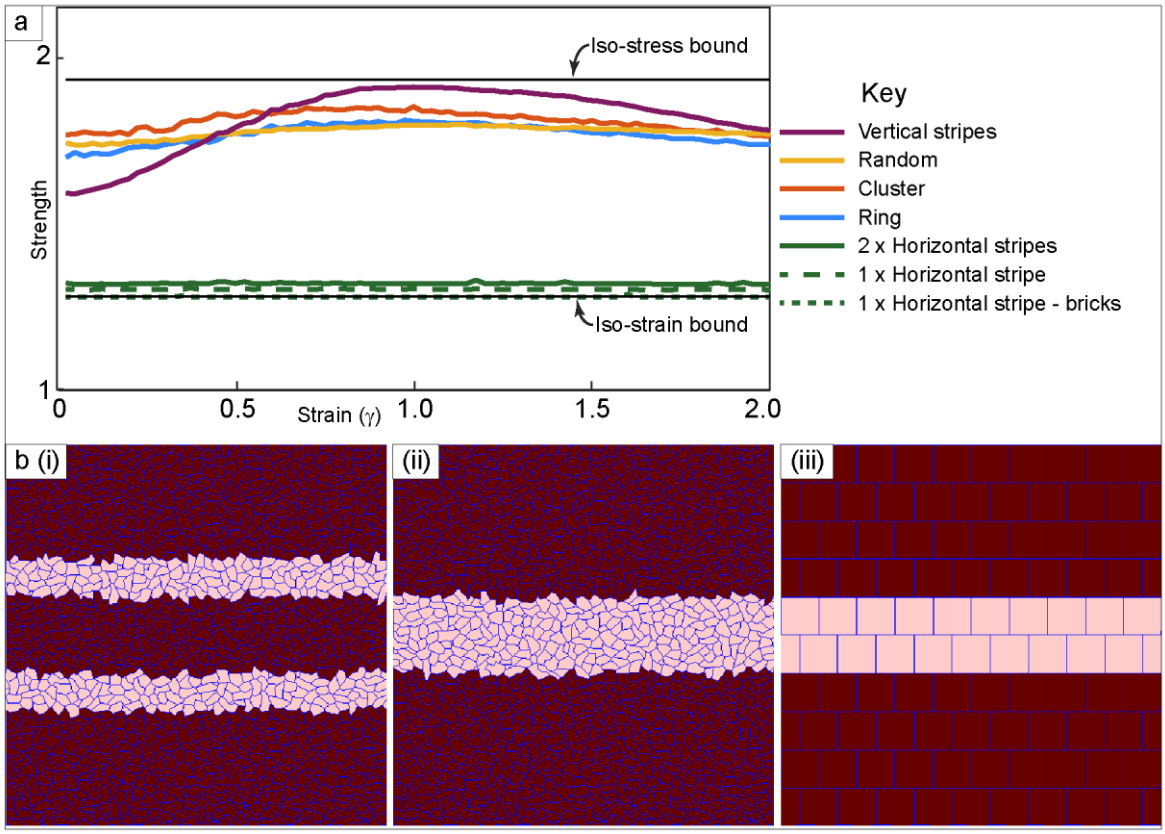

Supplementary Figure 2. (a) Simulation set I strength for Newtonian flow with iso-strain and iso-stress bounds plotted. (b) Striped geometries (i) two narrow stripes with irregular edges as used in the models; (ii) a single stripe with irregular edges (iii) a single stripe with smooth edges; strengths are plotted in (a).

Stress Exponent (n)	Strength of η = 1 control	Strength of η = 5 control
n = 1	0.46	2.30
n = 3	0.92	4.61

Supplementary Table 1. Values from the control models for weak and strong material used in iso-stress and iso-strain bound calculations.

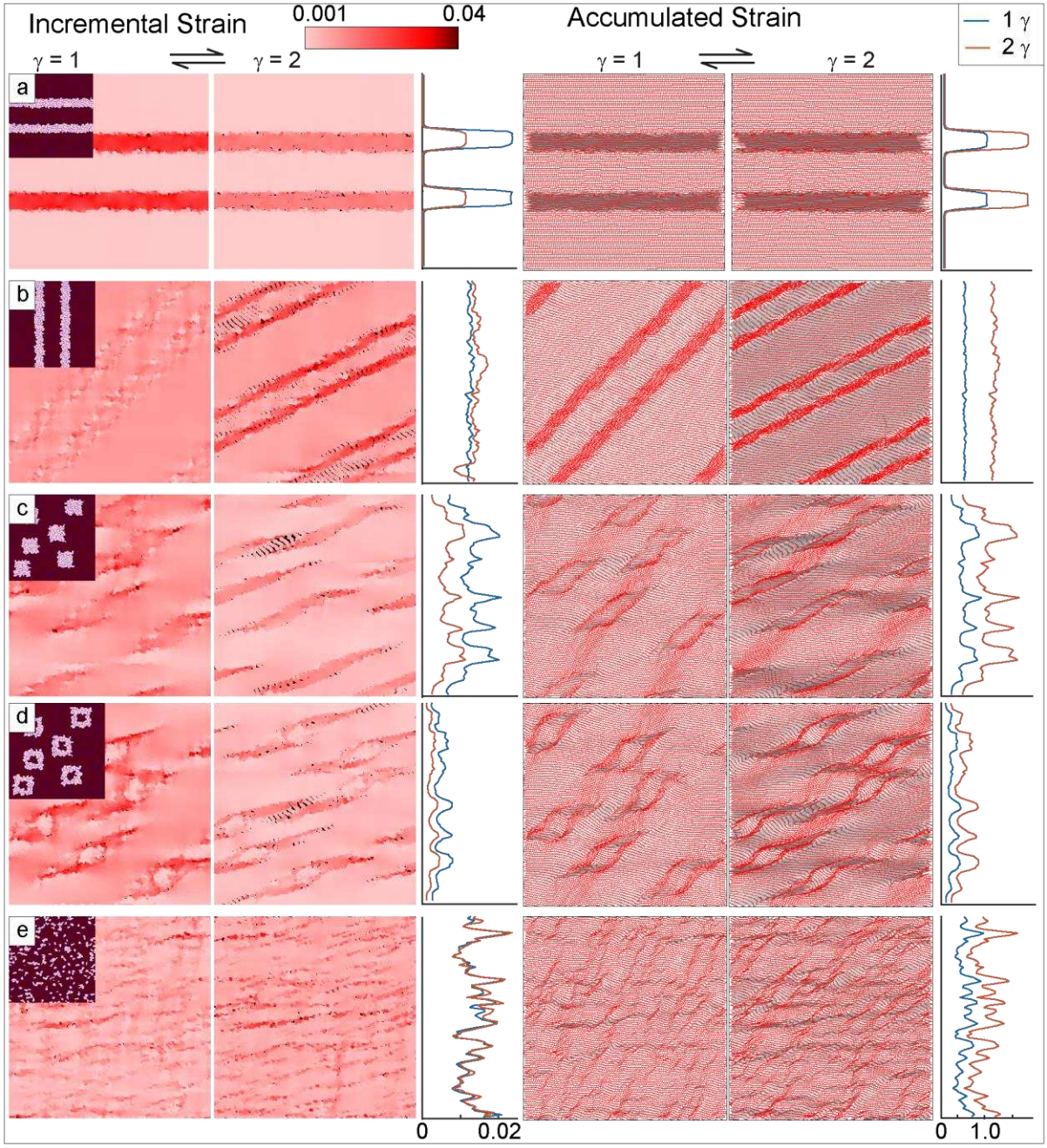

Supplementary Figure 3. Simulation set I: Strain localisation in the geometries for mixed flow properties. Interconnected weak layers (IWLs) have not formed by γ of 2. Pre-existing weak layers in horizontal geometry form IWLs.

Supplementary Figure 4. Field outcrop example of vertical striped geometry deformed by the development of a shear zone, from Pembroke Valley, New Zealand; photo courtesy Liene Spruzeniece.

Supplementary Movie Information:

For comparison purposes, all movies are run to a γ of 2.0. An additional movie, 3a continues movie 3 to γ of ~ 2.75 as discussed below. Please refer to Table 1 for specifics of the Simulations sets shown.

Movie 1: Simulation set III: Vertical stripe geometry with σ_{Thr} = 6.0 showing the development of an interconnected weak layer (IWL). Movie is of stress in the polygons. Brown areas are relatively higher stress. At ~ 10 seconds, the IWL is initiated with higher stress areas being converted to weak areas (which are pink), per the logic in Figure 1c. Once the IWL is formed the high stress (brown) polygons occur on the edges of the IWL, thereby making it wider as they are converted to weak polygons.

Movie 2: Simulation set III: Vertical stripe geometry with σ_{Thr} = 6.0. This is from the same run as for movie 1, but shows the incremental strain in the polygons.

Movie 3: Simulation set IV: Cluster geometry with σ_{Thr} = 5.0 and A_{Thr} = 15 showing deveopment of anatomosing IWLs. Movie is of incremental strain in the 100x100 square grid of unconnected nodes. The strain in the IWLs varies over time due to the logic in Figure 1d. The top narrow IWL, after initial formation, has progressively reduced strain concentration to γ of 2.0 (the end of movie 3).

Movie 3a shows movie 3 continued to γ of ~ 2.75. It shows by γ of ~ 2.5 the IWL is dormant, and no longer concentrating any strain.

Movie 4: Simulation set IV: Incremental strain in cluster geometry with $\sigma_{Thr} = 4.0$ and $A_{Thr} = 15$ for comparison with movie 3 to show impact of increased weakening (i.e. reduced stress threshold) – strain is more distributed.

Movie 5: Simulation set IV: Incremental strain in cluster geometry with $\sigma_{Thr} = 6.0$ and $A_{Thr} = 15$ for comparison with movie 3 to show impact of decreased weakening (i.e. increased stress threshold) – strain is more concentrated.

Movie 6: Simulation set IV: Incremental strain in cluster geometry with $\sigma_{Thr} = 5.0$ and $A_{Thr} = 5$ for comparison with movie 3 to show impact of increased strengthening (i.e. decreased age threshold) – increased strain variability in the IWLs.

Movie 7: Simulation set IV: incremental strain in cluster geometry with $\sigma_{Thr} = 5.0$ and $A_{Thr} = 10$ for the 100x100 square grid of unconnected nodes (movie 3), showing only those nodes where $\varepsilon_{Incr} > 0.06$ - strain in the IWLs varies over time.